(Online) ISSN 2712-0562
Sustainable Engineering and Innovation *Original Research*
Vol. 7, No. 2, 2025, pp.575-588
https://doi.org/10.37868/sei.v7i2.id645

Appropriate-technology pyramid solar still: Experimental performance and TRNSYS validation

B. E. Tarazona-Romero[1], A. D. Rincón-Quintero[2], M. A. Duran-Sarmiento[3], J. A. Ascanio-Villabona[4], C. L. Sandoval-Rodriguez[5]

[1-5] Research Group in Energy, Automation and Control Systems (GISEAC), Unidades Tecnológicas de Santander, Bucaramanga, Santander, Colombia

*Corresponding author E-mail: name.btarazona@correo.uts.edu.co

Received Aug. 30, 2025
Revised Nov. 2, 2025
Accepted Nov. 10, 2025
Online Dec. 1, 2025

Abstract

Water scarcity remains a global challenge that directly affects rural communities. The objective of this study is to design, build, and validate a pyramid-shaped solar distiller using appropriate technology for the decentralized supply of fresh water in Bucaramanga, Colombia. We combined a nine-day experimental campaign (April 1-9, 2025) with a TRNSYS (Type 66a-EES) simulation, evaluating two simulation models: a simplified energy balance model (MS01) and a variant that includes the efficiency of the Hottel-Whillier-Bliss (HWB) collector (MS02). Ambient temperature, direct normal irradiance (DNI), and four internal temperatures were measured every five minutes with calibrated sensors during the experimental process. The prototype reached tank/steam temperatures of 42-49 °C and produced 225-750 ml/day, with a total of 3,861 ml; the peak of 750 ml on a day of low irradiance was due to thermal inertia and reduced losses. Both simulation models reproduced the thermal and production trends with relative errors between ±0.012 and ±0.040. The cumulative yield on April 9 was 3765 ml (−2.5%) for MS01 and 3995 ml (+3.5%) for MS02. In summary, MS01 adjusted the tank/steam temperature values slightly better, while MS02 improved the distillation output prediction and offers greater calibration potential through the HWB parameters (FR, UL, (τα)e). The results indicate technical feasibility and scalability for rural contexts, and point to simple design improvements (sealing, leak control, thermal management) to increase daily production. Overall, passive desalination is a practical alternative.

Keywords: Appropriate technology, Hottel-Whillier-Bliss model, Passive desalination, Pyramid solar still, TRNSYS

1. Introduction

Water scarcity around the world has become a global challenge, threatening the health and survival of people, ecosystems, and the socioeconomic development of regions [1]. Driven mainly by population growth, technological development, increased urbanization, and climate change, it primarily affects arid regions [2]. According to a report presented in 2025 and developed jointly by the World Health Organization (WHO) and the United Nations Children's Fund (UNICEF), around 2.1 billion people worldwide lack access to safely managed drinking water. This shows an increase in global coverage from 50% to 60% in rural areas, while in urban areas, coverage reaches 83%. However, it points out that inequalities persist and that improvements in

access have been more pronounced in rural areas in relative terms, but much of the absolute progress has been in urban areas [3].

In Colombia, there are still big differences in access to clean water between urban and rural areas. According to a recent study [4], while around 98% of people in cities have access to water services, in rural areas this figure is only 73%, which is a gap of 25 percentage points. This situation, based on official data released by Colombia's National Administrative Department of Statistics (DANE) in the 2018 census, reflects the need to improve infrastructure and water resource management in rural areas, where 39.2% of households do not have an adequate quality supply, increasing their health and social vulnerability [5].

These water scarcity problems are exacerbated by inefficient resource management, pollution, and overexploitation of groundwater [6]. In this context, solar desalination, understood as the process of removing salt and other minerals from seawater or brackish water, is emerging as a promising strategy for ensuring access to drinking water [7]. In recent decades, these technologies have undergone remarkable advances that have improved their efficiency, reduced their costs, and strengthened their environmental sustainability, consolidating them as a key alternative to the water crisis [8]. Within this field, there are two main approaches: active and passive [9].

Active systems, although more efficient and with greater production capacity, require high investment and operating costs, which limit their implementation in rural communities. In contrast, passive technologies, such as pyramid solar stills (PSS), represent a viable option by directly harnessing solar energy for evaporation and condensation [10], with simple designs, low cost, and high adaptability to the concept of appropriate technology [11]. The latter refers to low-cost technical solutions that are easy to maintain, culturally accepted, and adapted to local conditions [7], making passive solar desalination a particularly suitable alternative for remote areas with limited resources [12].

Between 2022 and 2023, various studies explored improvements in pyramidal solar stills (PSS). Modi and Gami [13] used $NaNO_3$ and Al_2O_3 nanofluids as thermal storage materials, achieving 5.5% higher efficiency and lower costs with $NaNO_3$. Omara et al. [14] evaluated convex and dish absorbers, achieving 6.75 l/m²·day with costs of up to $0.015/l, while Ajit et al. [15] increased productivity by 40–73% using clay pots. Ahmed et al. [16] showed that PCM-encapsulated fins increased efficiency to 49.9% compared to 34.6% for conventional systems, and Shanmugan et al. [17] reported a yield of 4.28 l/m²·day and efficiency of 38.1% in a stepped PSS.

In 2024 and 2025, the trend toward hybrid systems with PCM and nanoparticles became established. Abed et al. [18] increased productivity by 117.6% with PCM, while Wei et al. [19] achieved 16.7% higher performance in floating systems with nanostructured coatings. Essa et al. [20] reported up to a 166% increase by combining triangular absorbers, reflectors, PCM, and solar tracking; Mekki et al. [21] showed that 2 kg of PCM optimized efficiency (32%) and reduced CO_2 emissions by 11.1 t; and Meena et al. [22] integrated vacuum tube collectors, PCM, and fins, reducing costs to $0.0094/l. However, this work focuses on the development of a pyramidal system with materials accessible in the region of Bucaramanga, Santander, designed for application in rural environments, where the local availability of inputs facilitates its construction, maintainability over time, and validation using a mathematical simulation model implemented in TRNSYS.

2. Methods and materials

2.1. Experimental setup

In this study, a pyramidal solar distiller was designed and developed based on the concept of appropriate technology, consisting of a single tank to carry out the experimental phase and estimate the amount of water generated. Figure 1A shows a side view of the system, where its characteristic pyramidal shape can be seen. The sloping cover with a maximum height of 441 mm is noteworthy, suggesting an angle that favors the condensation of water vapor on the inner walls and its subsequent collection at the lower edges. The base has a length of 1014 mm, confirming that the system maintains a square or almost square structure in plain view. In

general terms, the structure is divided into three parts: a lower area of 134 mm that acts as a saltwater reservoir, an intermediate section of 174.07 mm that provides support and thermal stability, and a 441 mm pyramidal cover designed to maximize solar capture and promote the condensation of fresh water on its internal walls.

For your part, Figure 1 B shows the plan view of the system, which has a square base measuring 1124.17 mm x 1124.17 mm. The presence of diagonal X-shaped reinforcements suggests a structural design optimized to improve the mechanical strength of the system and possibly support a sloped roof. In addition, the dimensions of 560 mm x 560 mm within the main area could indicate subdivisions to optimize condensed water collection or improve thermal distribution inside the still. The inclusion of rounded corners in the structure may be a design strategy that minimizes mechanical stress and facilitates the drainage of distilled water, reducing losses due to secondary evaporation.

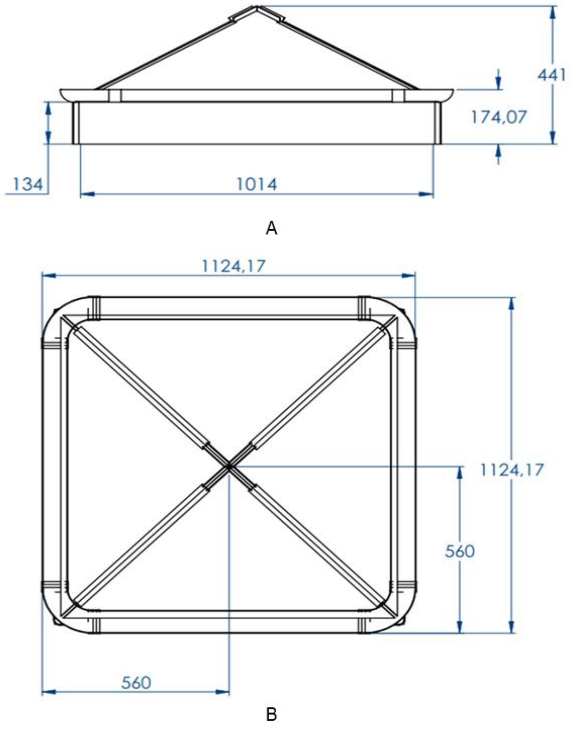

Figure 1. Side view (A) and plan view (B) of the pyramidal solar distiller designed under the concept of appropriate technology. Note: Own elaboration. Unit values expressed in millimeters (mm)

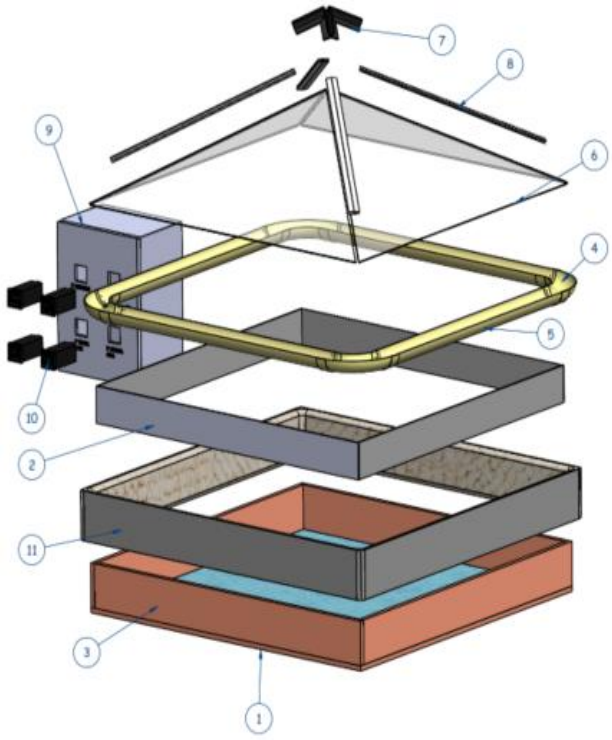

Figure 2. Exploded view of the pyramidal solar still designed in 3D CAD

Figure 2 shows an exploded view of the pyramidal solar still. At the bottom is the baseboard (1), accompanied by the thermal insulation fabric (11) and the wooden side boards (3) that make up the body of the system. In the middle are the mirrors (2) and mirror separators (8), whose function is to reflect solar radiation inward. The upper part consists of PVC pipes (5), PVC elbows (4), the triangular pyramid glass (6), and the upper angles (7) that reinforce the structure, while the electrical box (9) and pyrometers (10) allow for the monitoring of thermal variables.

A total of 11 materials were used, six of which correspond to the system's own structure, and five were purchased on the market. Most are counted by units, while three are measured in meters (PVC pipe, mirror separator, and insulating fabric). The design integrates wood, glass, and mirrors as structural materials, along with functional components such as PVC and insulation, achieving a balance between local manufacturing and commercial procurement. Likewise, the incorporation of the electrical box (9) and pyrometers (10) shows that the system is geared toward both solar desalination and experimental validation of its performance.

Additionally, Table 1 presents the thermophysical properties of the materials, which are necessary for accurate modeling in the TRNSYS simulation phase.

Table 1. Thermophysical properties for simulation in TRNSYS (reference values at ~20–25 °C)

Material	k (W/m·K)	c_p (J/kg·K)	ρ (kg/m³)	Source
Glass	1.05	840	2500	[23]
Saltwater	0.60	3990	1025	[24]
Madera (base)	0.12	1700	600	[25]
XPS insulation	0.035	1400	30–45	[26]
Interior air	0.026	1005	1.2	[27]

2.2. Experimental method

The experimental campaign was carried out at the Santander Technological Units, where hourly measurements of temperature and solar radiation were taken on eleven consecutive days between April 1 and 9, 2025. To this end, four temperature sensors were placed at strategic points in the passive solar desalination system (collector outlet, inside the tank, steam-water zone, and surrounding environment), in addition to a calibrated pyranometer to record incident solar radiation. Figures 3A and B show the installation of the system and the layout of the measuring instruments.

The data obtained were systematically organized and tabulated with a recording frequency of 5 minutes, which allowed for the analysis of daily thermal patterns, the identification of direct correlations with solar radiation, and the detection of possible thermal delays between the different monitored areas. This information constitutes the experimental basis necessary for the subsequent validation of the simulation model, ensuring its consistency with actual operating conditions.

A B

Figure 3. Side view (A) and low-angle view (B) of the pyramidal solar distiller built according to the concept of appropriate technology

It underwent a verification process at the Industrial Instrumentation Laboratory to determine the errors. This process was carried out using a Presys TE-25N dry block and a 4-wire PT100 reference resistance. The differences in readings obtained in the 16 measurements between each test sensor and the standard value were interpreted in terms of error propagation, considering the uncertainties associated with both the reference and the measured sensors. Table 1 shows the average errors calculated for each sensor, together with the identification of the type of sensor used (K-type or J-type thermocouple), which allows the systematic trend of each device to be analyzed.

Table 2. Average sensor errors

Sensor	Range	Accuracy	Error (°C)
Sensor 1 (Type K thermocouple) Distiller outlet	(0 – 100)	+/- 1 °C	+0,333
Sensor 2 (Type J thermocouple) Storage tank	°C	+/- 1.23 °C	–0,417
Sensor 3 (Type J thermocouple) Wet steam (inside the pyramid)			–0,417
Sensor 4 (Type J thermocouple) Ambient			–0,417

In general terms, the overall propagation of error was expressed as:

$$\epsilon_T = \sqrt{\epsilon^2{}_{sensor} + \epsilon^2{}_{test}} \quad (1)$$

Where:

ϵ_{sensor} is the systematic deviation observed for the sensor with respect to the standard

ϵ_{test} corresponds to the uncertainty associated with the reference PT100 and the dry block

2.3. Mathematical models

This section presents the mathematical models used in the development of the simulation model, which are summarized in Table 3 and form the basis for estimating energy flows, thermal losses, and system productivity. In particular, two main formulations were used: the first corresponds to a simplified energy balance scheme that integrates the equations of absorption, convection, radiation, and instantaneous thermal efficiency; while the second introduces a variation based on Equation 9, the Hottel–Whillier–Bliss (HWB) model, widely used for flat-plate collectors [28]. This adaptation allowed for the incorporation of more robust parameters such as the removal factor, the overall loss coefficient, and the effective optical yield, thus achieving a more accurate and calibratable approximation of experimental conditions.

Table 3. Thermodynamic mathematical models

Name	Equation		Components/meaning
Absorbed solar gain	$Q_{sun} = G\ A\ \tau\ \alpha$	(2)	Q_{sun} absorbed heat (W) G irradiance (W/m²) A projected area (m²) τ transmittance α absorptance
Exterior convective coefficient (v≤5 m/s)	$h_{conv} = 2.8 + 3u$	(3)	h_{conv} external convection (W/m²·K) u wind speed (m/s)
Exterior convective coefficient (general)	$h = \begin{cases} 2.8 + 3\,u & si\ u \le 5\ m/s \\ 6.15\ u^{0.8} & si\ u \ge 5\ m/s \end{cases}$	(4)	h convection coefficient (W/m²·K)
Convection losses (indoor–room) (5)	$Q_{conv} = h_{conv}\ A\ (T_{int} - T_{ext})$	(5)	Q_{conv} convection losses (W) T_{int} internal temperature (°C) T_{ext} external temperature (°C)
Radiation losses (indoor–room)	$Q_{rad} = \varepsilon\ \sigma\ A\ (T^4{}_{int,K} - T^4{}_{ext,K})$	(6)	Q_{rad} radiation losses (W) ε emissivity σ Stefan–Boltzmann constant 5.67×10^(-8) (W/m²·K⁴)
Net useful heat (evaporation)	$Q_{evap} = Q_{sun} - Q_{conv} - Q_{rad}$	(7)	Q_{evap} net useful heat (W)

Name	Equation		Components/meaning
Instantaneous thermal efficiency (simple method)	$\eta = 100\ \frac{Q_{evap}}{Q_{sun}}$	(8)	η thermal efficiency (%)
Hottel-Whillier-Bliss HWB model [28] (plate collector)	$\eta_{HWB} = F_R\left((\tau\ \alpha\ )_e \frac{U_L(T_{int} - T_{ext})}{G}\right)$	(9)	η_{HWB} efficiency (%) F_R removal factor $(\tau\ \alpha\ )_e$ effective optical performance U_L global losses (W/m²·K)
Desalinator thermal efficiency	$e = \frac{\sum m\ \gamma}{3.6\ \sum A_a\ G}$	(10)	e efficiency (%) m hourly output (kg/h); γ latent heat of steam (kJ/kg) A_a absorber area (m²)
Brine energy balance	$\tau\alpha_w GA + q_k A_k = (q_e + q_c + q_r)A + M_w C_{pw}\frac{dT_w}{dt}$	(11)	α_w brine absorptance q_k, q_e, q_c, q_r heat fluxes (W/m²) M_w brine mass (kg) C_{pw} specific heat (J/kgK)
Evaporative heat flux	$q_e = 14.4 * 10^{-3}(\hat{P}_w - P_c)\left[T_w - T_g\frac{(\hat{P}_w - P_c)T_w}{268.9 * 10^{-3} - \hat{P}_w}\right]^{1/3}$	(12)	q_e evaporation flux (W/m²) $\hat{P}_w, P_c$ partial pressures (Pa) T_w, T_g temperatures (K)
Hourly productivity	$m = \frac{3.6\ q_e\ A}{\gamma}$	(13)	m hourly production (kg/h) q_e evaporation flow (W/m²)
Total production	$p = \sum_0^{t_s} m$	(14)	p total production (kg) t_s operating time (h)
Roof-to-Ambient Convection	$q_{gc} = h\ (T_g - T_a)$	(15)	q_{gc} roof-to-air convection losses (W/m²) h convection coefficient (W/m²·K) T_g roof temperature (K) T_a air temperature (K)
Roof-to-Sky/Ambient Radiation	$q_{gr} = \sigma\varepsilon_g\ ((T_g^4 - T_a^4) + (T_g^4 - T_s^4)$	(16)	q_{gr} roof radiation losses (W/m²) ε_g roof emissivity
Mass Balance (Overall)	$\dot{m}_{in} = \dot{m}_{out} + \dot{m}_{evap}$	(17)	$\dot{m}_{ini}$ initial mass (kg) $\dot{m}_{out}$ final mass (kg) $\dot{m}_{evap}$ evaporating mass (kg)
Vapor Partitioning	$\dot{m}_{evp} = \dot{m}_{cond} + \dot{m}_{perd}$	(18)	$\dot{m}_{cond}$ useful condensate (kg) $\dot{m}_{perd}$ losses (kg)
Average Factor (mL/°C)	$Factor_d = \frac{Producción_{exp}(d)}{T3_{exp} - T_{amb}(d)}$	(19)	$T3_{exp}\ (d)$ $t$temperature experienced by steam on the day $T_{amb}(d)$ experimental ambient temperature on the day $Factor_d$ indicating how much water is produced per degree of thermal difference

Name	Equation		Components/meaning
Water Production	$Producción_{mod}(d) = Factor_{prom}(T3_{mod}(d) - T_{amb}(d))$	(20)	$T3_{mod}(d)$ temperature experienced by steam during the day $Factor_{prom}$ which indicates how much water is produced for each degree of thermal difference

Note: Own creation. Source: [29] [30] [31] [32] [33]

2.4. Simulation model in TRNSYS

The passive solar desalination model was developed in the TRNSYS environment using code written in Engineering Equation Solver (EES), linked via the Type66a component. This code was based on the mathematical models described above and included two main formulations: the first, a simplified energy balance scheme that integrates the equations of absorption, convection, radiation, and instantaneous thermal efficiency; and the second, a variant that incorporates the Hottel–Whillier–Bliss (HWB) model applied to flat-plate collectors [28]. Figure 4 presents the structure of the simulation, in which climate data (Type9c) feeds the numerical module in EES (Type66a), and the results are displayed in Type65d, allowing dynamic analysis of thermal behavior and desalinated water production under representative meteorological conditions.

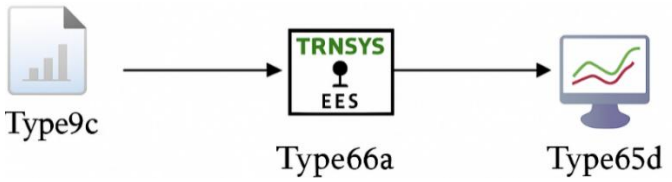

Figure 4. Block diagram of the passive solar desalination system simulation in TRNSYS through integration with EES

2.5. Validation of simulation models

The validation of the simulation models implemented in TRNSYS was performed by estimating absolute and relative errors, comparing the simulation outputs with the experimental reference data. Table 4 presents the mathematical models used to estimate each error.

Table 4. Mathematical models for estimating relative and absolute errors

Error name	Formula		Variable description
Absolute error	$EA = \lfloor X_{sim} - X_{exp} \rfloor$	(21)	X_{sim} value obtained from the simulation with TRNSYS X_{exp} experimental value EA absolute error ER relative error n total number of data points considered in the validation MEA mean absolute error MER mean relative error
Relative error	$ER = \frac{\lfloor X_{sim} - X_{exp} \rfloor}{X_{exp}}$	(22)	
Average absolute error	$MEA = \frac{1}{n}\sum_{i=1}^{n}\lfloor X_{sim} - X_{exp} \rfloor$	(23)	
Average relative error (24)	$MER = \frac{1}{n}\sum_{i=1}^{n}\frac{\lfloor X_{sim} - X_{exp} \rfloor}{X_{exp}}\ x\ 100$	(24)	

Note: Own creation. Source [34] [35]

3. Results and discussion

It is important to understand the influence of direct normal irradiation (DNI) and ambient temperature when determining the efficiency of solar distillers. These two variables have a significant impact on the efficiency and productivity of this type of system. Figure 5 shows the ambient temperature and DNI recorded during the

experimental process. These values were also used in the evaluation process of the simulation models developed. In general terms, high ambient temperatures tend to increase the evaporation rate, resulting in greater heat losses. For its part, DNI is responsible for supplying the energy needed to carry out the distillation process. When DNI is prolonged over time, it directly influences heat transfer and evaporation rates within the still.

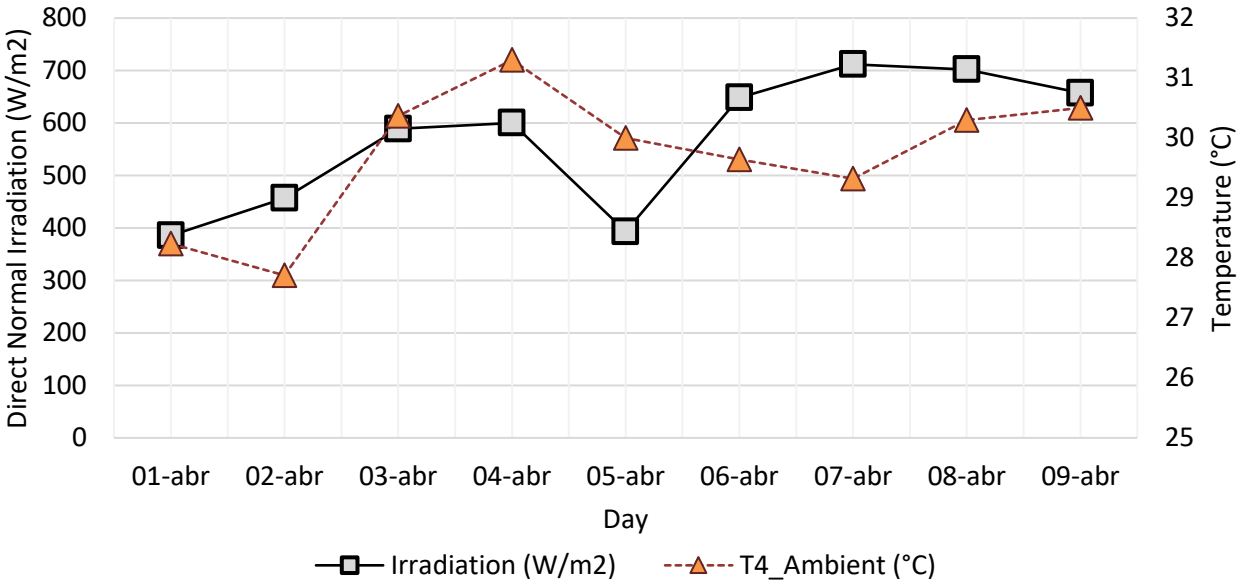

Figure 5. Daily variation of direct irradiance and ambient temperature on the days of experimentation

Figure 6 shows the results obtained in the experimental phase of the solar distillation system, where the evolution of the temperatures recorded between April 1 and April 9 can be observed. It can be seen that the system output (T1_Out) has the lowest values, stabilizing at around 30 °C after an initial peak of 42 °C, reflecting possible heat losses or limited heat exchange at that point. On the other hand, the tank temperature (T2_Tank) and the steam temperature (T3_Steam) show greater stability, reaching between 42 and 49 °C, with a clear consolidation from April 6 onwards, when the system begins to operate more efficiently. The fact that the steam exceeds the tank in the last few days shows better use of the DNI and a favorable thermal gradient for condensation, which translates into greater distilled water production.

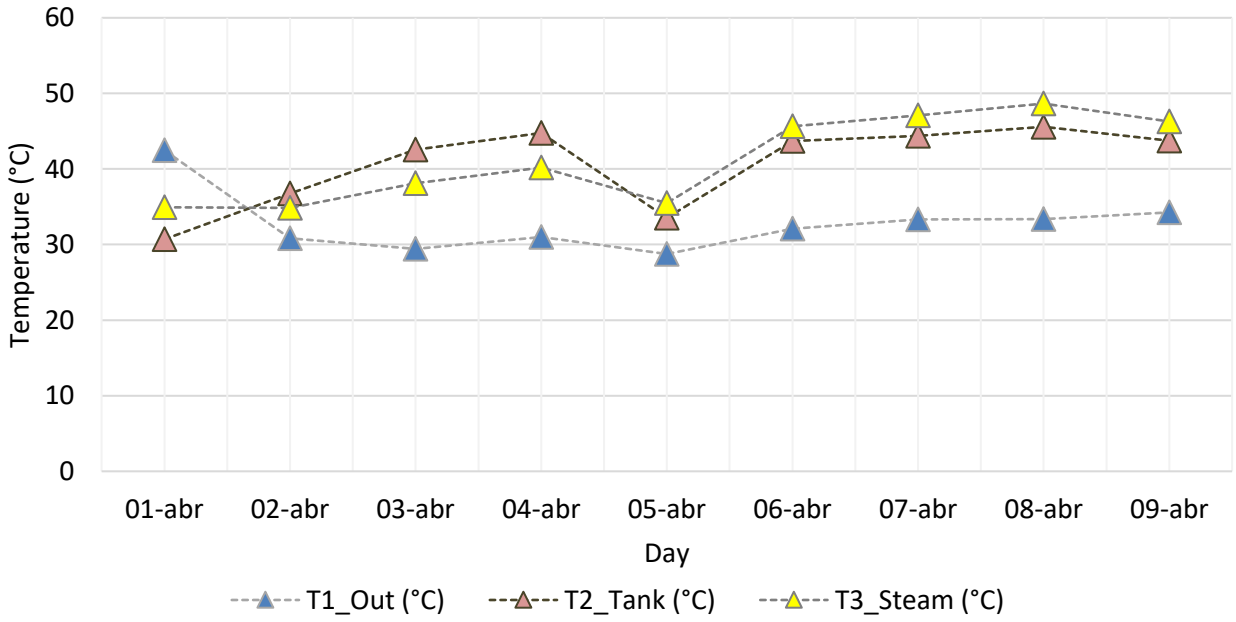

Figure 6. Temporal variation of temperatures recorded in the solar distiller probes

Figure 7 shows the daily water production in mL and the cumulative production during the experimental phase of the solar distiller. It can be seen that the evolution of distilled water production is directly linked to temperature and solar radiation behavior. During the first few days (April 1 to 3), system temperatures (outlet, tank, and steam) remained moderate, accompanied by relatively low radiation levels, which is reflected in limited daily production between 225 and 415 mL. From April 4 onward, increased radiation raised the tank and steam temperatures (close to 45–49 °C), while on April 5, despite being a day with low irradiance, maximum production was reached with 750 mL, explained by the thermal inertia of the system and conditions of high radiation. °C), while on April 5, despite being a day with low irradiance, maximum production peaked at 750 mL, explained by the thermal inertia of the system and favorable conditions such as lower heat loss and higher initial temperatures.

Subsequently, although temperatures continued to rise and radiation remained relatively stable, production fluctuated (345–520 mL), demonstrating that factors such as ambient temperature, energy accumulation, and heat loss also influence production in addition to irradiance. Taken together, Figures 7 and 5 show that the distillation system responds positively to increases in radiation and temperature, but also to cumulative effects, achieving a total production of 3861 mL.

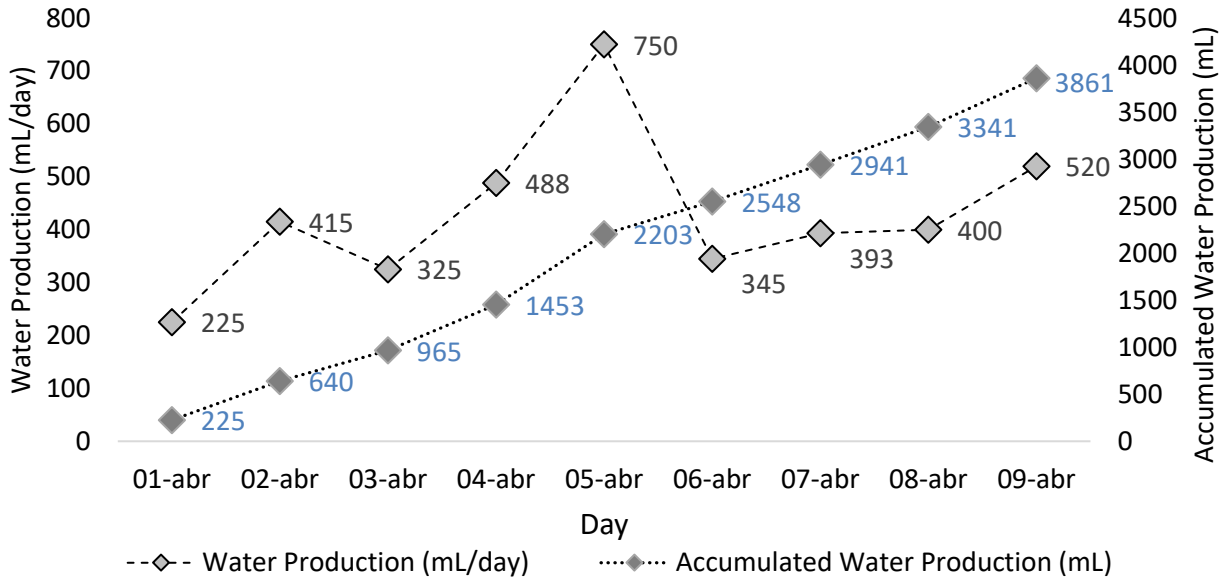

Figure 7. Water production per day and accumulated in the solar distiller in the experimental phase

Table 4 compares the experimental temperature values (outlet, tank, and steam) with those obtained in the MS01 and MS02 simulation models. In general, both models adequately reproduce the trends observed in the experimental phase, with minimal differences in most cases. For the outlet temperature, MS01 tends to slightly underestimate the experimental values, while MS02, by incorporating the Hottel–Whillier–Bliss (HWB) model, offers a better approximation at several points, more accurately reflecting the dynamics of global losses and the optical performance of the plate collector. In the case of the tank, both models follow the upward behavior recorded experimentally, although MS01 is numerically closer. In the vapor zone, the simulations capture the upward trend until it exceeds 45 °C, with MS01 adjusting better at the maximum values and MS02 showing a more conservative prediction.

Table 4. Comparison of thermal variables between experimentation and simulation (MS01 and MS02)

Experimentation			Simulation model 01 (MS01)			Simulation model 02 (MS02)		
Out (°C)	Tank (°C)	Steam (°C)	Out (°C)	Tank (°C)	Steam (°C)	Out (°C)	Tank (°C)	Steam (°C)
42,47	30,7	34,92	44,139	32,137	36,347	40,771	31,117	35,853
30,83	36,77	34,85	30,374	37,319	35,42	31,958	35,299	34,544

Experimentation			Simulation model 01 (MS01)			Simulation model 02 (MS02)		
29,43	42,57	38,1	28,649	43,571	39,155	30,607	40,867	36,889
30,98	44,74	40,2	30,142	45,813	41,338	32,219	43,85	38,81
28,75	33,54	35,5	28,417	33,957	35,917	29,525	34,882	34,08
32,1	43,69	45,65	31,058	44,976	47,176	33,384	41,942	43,824
33,31	44,37	47,09	31,978	45,985	48,974	34,642	45,781	45,206
33,36	45,58	48,65	32,073	47,171	50,596	34,694	46,808	46,704
34,27	43,76	46,29	33,137	45,096	47,895	35,641	45,51	44,438

Table 5, which presents the absolute and relative errors, allows these observations to be quantified. At the outlet, the absolute error of MS01 reaches up to ±1.6 °C, while in MS02, the deviations are reduced and remain close to ±1.3 °C, which shows a better prediction of this parameter in MS02. In the tank, both models show relative errors of around ±0.04, although MS01 tends to offer a more stable fit. In the vapor, the two models record similar errors, with slight advantages for MS01 at high values. Overall, the relative errors, which range between ±0.012 and ±0.040, confirm that the approximation of both models is satisfactory, but that the inclusion of the HWB model in MS02 provides greater realism in the simulation of the outlet temperature, at the cost of slight discrepancies in the tank and steam.

Table 5. Comparative analysis of simulation errors (MS01 and MS02)

Absolute Error-MS 01			Absolute Error MS 02			Relative Error MS 01			Relative Error MS 02		
Out (°C)	Tank (°C)	Steam (°C)	Out (°C)	Tank (°C)	Steam (°C)	Out	Tank	Steam	Out	Tank	Steam
1,669	1,437	1,427	-0,699	0,417	0,933	0,039	0,047	0,041	-0,016	0,014	0,027
-0,456	0,549	0,570	1,128	-1,471	-0,306	-0,015	0,015	0,016	0,037	-0,040	-0,009
-0,781	1,001	1,055	1,177	-1,703	-1,211	-0,027	0,024	0,028	0,040	-0,040	-0,032
-0,838	1,073	1,138	1,239	-0,890	-1,390	-0,027	0,024	0,028	0,040	-0,020	-0,035
-0,333	0,417	0,417	0,775	1,342	-1,420	-0,012	0,012	0,012	0,027	0,040	-0,040
-1,042	1,286	1,526	1,284	-1,748	-1,826	-0,032	0,029	0,033	0,040	-0,040	-0,040
-1,332	1,615	1,884	1,332	1,411	-1,884	-0,040	0,036	0,040	0,040	0,032	-0,040
-1,287	1,591	1,946	1,334	1,228	-1,946	-0,039	0,035	0,040	0,040	0,027	-0,040
-1,133	1,336	1,605	1,371	1,750	-1,852	-0,033	0,031	0,035	0,040	0,040	-0,040

Figure 8 compares the daily distilled water production between the experimental data and the results of the MS01 and MS02 simulation models. In the first few days (April 1 to 3), the differences are small and remain below ±12 mL/day, representing only between 2% and 5% of the actual value produced. This behavior allows us to consider these discrepancies as minimal, since they do not affect the general trend or the level of accuracy of the models. Both MS01 and MS02 consistently follow the evolution of the experimental curve, showing that they are reliable tools for describing the performance of the system under relatively stable radiation and temperature conditions.

From April 4 onwards, the differences begin to grow, becoming more noticeable on April 5 and 7, when the largest errors occur. MS01 maintains a tendency to underestimate production, with errors reaching –17 mL/day on April 9, while MS02 tends to overestimate it, reaching a maximum of 26.8 mL/day on April 5 and 20.8 mL/day on April 9. April 7 is the most critical day, with errors close to 15 mL/day in both models, as highlighted in the zoomed area. Despite these differences, the simulations retain the shape and trend of the experimental curve, confirming that the two models adequately represent the dynamics of the system. However, when considering the mathematical structure, MS02, by incorporating the Hottel–Whillier–Bliss model, offers a more robust and flexible framework for calibration, making it the model with the greatest potential for adjustment with respect to the experimental results.

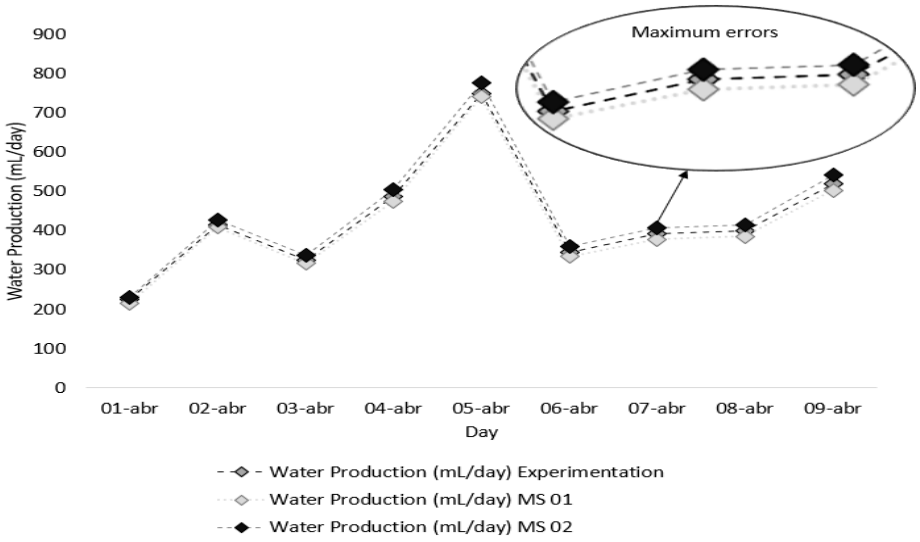

Figure 8. Daily water production in experiments and simulations (MS01, MS02)

Finally, Figure 9 shows the comparison between the cumulative distilled water production obtained experimentally and that estimated using the MS01 and MS02 simulation models. In general terms, the three curves show progressive growth and are very close to each other, which shows that the models adequately reproduce the accumulation trend observed in practice. From the early days, the differences are minimal, less than 30 mL, reflecting a good level of prediction in low-production scenarios. As the experimental period progresses, discrepancies tend to increase, especially after April 5. At the close of April 9, cumulative experimental production reached 3,861 mL, while MS01 predicted 3,765 mL, and MS02 reached 3,995 mL. This confirms that MS01 maintains a more conservative behavior, slightly underestimating the results, while MS02 tends to overestimate them. However, the final differences do not exceed ±3.5% of the experimental value, which is considered acceptable in this type of study.

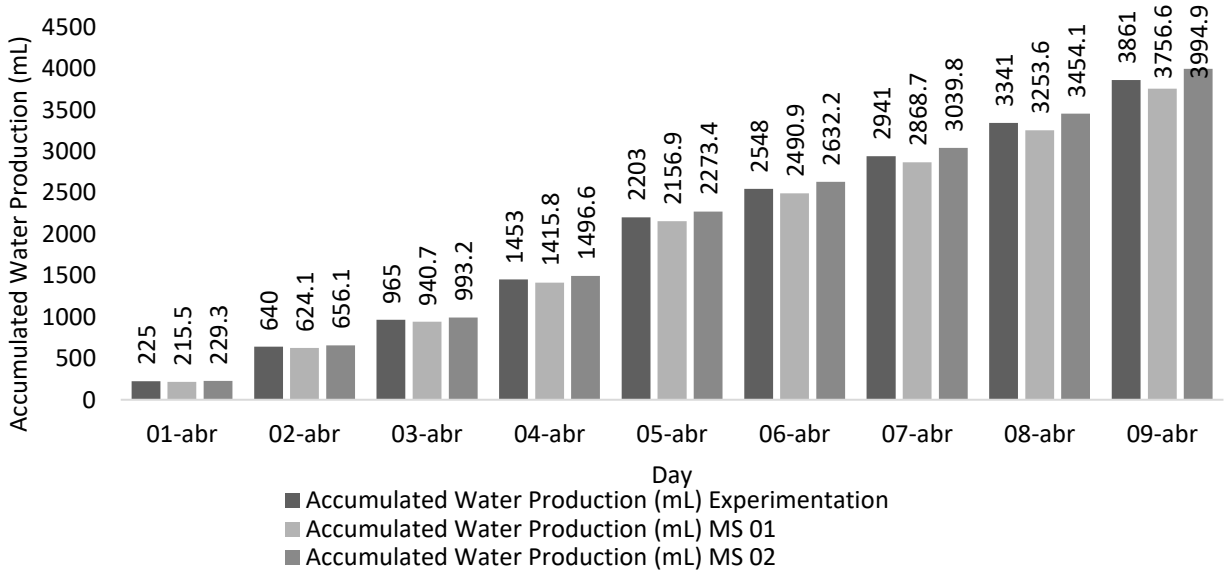

Figure 9. Accumulated water production: experimentation vs. simulated models (MS01 and MS02)

4. Conclusions

This study integrated experimentation and mathematical modeling in TRNSYS (Type66a + EES) to evaluate the performance of a pyramidal solar distiller developed under the paradigm of appropriate technology, considering the joint influence of ambient temperature and direct normal irradiation (DNI) on thermal behavior

and water production. In the experimental phase, the system reached tank and steam temperatures between 42–49 °C and a daily production of 225–750 mL, with a cumulative total of 3861 mL. The maximum of 750 mL was obtained on a day of low irradiance, due to thermal inertia and lower losses; on the other hand, the 7th day of testing showed the greatest discrepancy between measurements and simulations.

Productivity increased with the rise in effective internal temperature (difference between vapor temperature and ambient temperature) and with sustained energy availability (DNI). Beyond solar resources, operational factors such as previous thermal conditions, convection and radiation losses, and brine volume affected performance, resulting in fluctuations of 345–520 mL/day in the final days of the test. These results confirm the system's sensitivity to both environmental variables and operational and design decisions.

The simulation models adequately reproduced the thermal and production trends observed in the experimental phase. Overall, relative errors remained between ±0.012 and ±0.040, indicating an acceptable level of agreement for prototype-scale validation. By variable, simulation model 01 used a simplified energy balance and showed a better fit for tank and steam temperatures than simulation model 02. On the other hand, the latter, by incorporating the Hottel–Whillier–Bliss (HWB) model, offered a more accurate estimate of the output, explicitly considering overall losses (U_L) and optical performance (τα). In terms of cumulative production, simulation model 01 underestimated by −2.5% (3,765 mL) and simulation model 02 overestimated by +3.5% (3,995 mL) compared to the experimental value (3,861 mL), differences that are within acceptable ranges for this type of simulation.

While simulation model 01 offered a more conservative and stable prediction, simulation model 02 provided a more robust and calibratable physical framework, with FR, UL, and (τα)e parameters, allowing for better adjustment to new environmental or operating conditions while maintaining fidelity to the heat transfer mechanisms of the flat plate collector. From an appropriate technology perspective, the pyramidal distiller demonstrated technical feasibility and potential for implementation in rural contexts by combining local construction (wood, glass, PVC, insulation) with basic instrumentation for operation and monitoring; its performance can be enhanced with improvements in sealing, loss control, and thermal management.

Finally, the following future work is proposed: formal calibration of simulation model 02 using multi-parameter optimization (FR, UL, (τα)e); seasonal evaluation with long series of DNI and wind data; exergy and levelized cost per liter analysis; and study of passive strategies (reflectors and PCM) to increase daily production without sacrificing simplicity and maintainability. These lines of work will consolidate the maturity of the model and the transferability of the prototype to real rural scenarios.

Declaration of competing interest

The authors declare that they have no known financial or non-financial competing interests in any material discussed in this paper.

Funding information

No funding was received from any financial organization to conduct this research.

Acknowledgements

Special thanks to the Unidades Tecnológicas de Santander for their support in this research.

Author contribution

The contribution to the article is as follows: B. E. Tarazona-Romero was responsible for the conception, design, and overall coordination of the study; A. D. Rincón-Quintero conducted the experimental setup and data collection; M. A. Durán-Sarmiento participated in the TRNSYS modeling and numerical simulations; J. A. Ascanio-Villabona contributed to the analysis and interpretation of results; and C. L. Sandoval-Rodríguez

prepared the first draft of the manuscript and supported the final editing process. All authors discussed the results, reviewed the manuscript critically, and approved the final version.

References

[1] R. Safoui *et al.*, «Atmospheric water harvesting using a desiccant-based solar still: experimental investigation and economic analysis», *Eng. Res. Express*, vol. 6, n.º 4, p. 045559, dic. 2024, https://doi.org/10.1088/2631-8695/ad970a

[2] K. Ramzy, M. Abdelgaleel, and E. A. abdelAziz, «Assessment the pyramid solar still performance using PCM, thermoelectric coolers, and optical lenses: Energy, exergy efficiency, economic and environmental impact», *International Communications in Heat and Mass Transfer*, vol. 168, p. 109419, nov. 2025, https://doi.org/10.1016/j.icheatmasstransfer.2025.109419

[3] OMS y UNICEF, «Progress on household drinking water, sanitation and hygiene 2020-2024», Organización Mundial de la Salud (OMS/WHO) y Fondo de las Naciones Unidas para la Infancia (UNICEF)., Ginebra, Suiza., 2025. [En línea]. Disponible en: https://www.unicef.org/rosa/press-releases/fast-facts-1-4-people-globally-still-lack-access-safe-drinking-water-who-unicef?utm_source=chatgpt.com

[4] A. Y. B. Pedraza y W. L. Calpe, «Transformaciones en el espacio urbano-rural en Colombia y su impacto en el suministro de agua», *Territorios*, n.º 50, 2024, https://doi.org/10.12804/revistas.urosario.edu.co/territorios/a.12222

[5] DANE, «Censo Nacional de Población y Vivienda 2018», Departamento Administrativo Nacional de Estadística (DANE), Bogota, Colombia, 2018.

[6] B. K. Mishra, P. Kumar, C. Saraswat, S. Chakraborty, and A. Gautam, «Water Security in a Changing Environment: Concept, Challenges and Solutions», *Water*, vol. 13, n.º 4, p. 490, ene. 2021, https://doi.org/10.3390/w13040490

[7] B. E. Tarazona-Romero, A. Campos-Celador, and Y. A. Maldonado-Muñoz, «Can solar desalination be small and beautiful? A critical review of existing technology under the appropriate technology paradigm», *Energy Research & Social Science*, vol. 88, p. 102510, jun. 2022, https://doi.org/10.1016/j.erss.2022.102510

[8] B. E. Tarazona-Romero, A. Meneses-Jácome, Y. A. Maldonado-Muñoz, y A. Campos-Celador, «Solar Desalination and the Application of the Life Cycle Analysis Method: A Mini-Review», en *The Circular Bioeconomy in Industry: Strategies for Sustainable Resource Recovery, Environmental Balance, and Ecosystem Protection*, A. Meneses-Jácome, U. Schmid-Staiger, y T. C. Guarín C., Eds., Cham: Springer Nature Switzerland, 2025, pp. 135-139. https://doi.org/10.1007/978-3-031-84359-4_21

[9] V. Dogra, C. Kishore, A. Verma, and J. Gupta, «Active and Passive Solar Distillation—A Detailed Review», en *Polymer Composites: From Computational to Experimental Aspects*, S. K. Sethi, H. S. Gupta, and A. Verma, Eds., Singapore: Springer Nature, 2024, pp. 383-412. https://doi.org/10.1007/978-981-97-0888-8_19

[10] S. Kumar *et al.*, «Solar stills: A review for water scarcity solutions», *Heliyon*, vol. 10, n.º 19, p. e38751, Oct. 2024, https://doi.org/10.1016/j.heliyon.2024.e38751

[11] E. Pallares-Carballo, B. E. Tarazona-Romero, J. G. Ascanio-Villabona, y O. Lengerke-Pérez, «Centro de Investigación de la Universidad Distrital Francisco José de Caldas», *Visión electrónica*, vol. 19, n.º 1, jun. 2025, Accedido: 24 de septiembre de 2025. [En línea]. Disponible en: https://revistas.udistrital.edu.co/index.php/visele/article/view/23789

[12] S. Tanzim, Md. M. Alam, T. K. Shailo, and S. U. Mahmud, «Construction and Feasibility Investigation of a Small-Scale Single-Basin Solar Still for Remote Areas», in *2024 International Conference on Innovations in Science, Engineering and Technology (ICISET)*, Oct. 2024, pp. 1-4. https://doi.org/10.1109/ICISET62123.2024.10941656

[13] K. V. Modi y A. R. Gamit, «Investigation on performance of square pyramid solar still using nanofluid and thermal energy storage material: An experimental and theoretical study», *Journal of Cleaner Production*, vol. 381, p. 135115, dic. 2022, https://doi.org/10.1016/j.jclepro.2022.135115

[14] «Experimental study on the performance of pyramid solar still with novel convex and dish absorbers and wick materials», *Journal of Cleaner Production*, vol. 373, p. 133835, Nov. 2022, https://doi.org/10.1016/j.jclepro.2022.133835

[15] Ajit, H. Pandey, and N. Kumar Gupta, «Productivity analysis of pyramid solar still with solid clay pots», *Materials Today: Proceedings*, vol. 62, pp. 4081-4085, ene. 2022, https://doi.org/10.1016/j.matpr.2022.04.629

[16] M. E.A.E. Ahmed, S. Abdo, M. A. Abdelrahman, and O. A. Gaheen, «Finned-encapsulated PCM pyramid solar still – Experimental study with economic analysis», *Journal of Energy Storage*, vol. 73, p. 108908, dic. 2023, https://doi.org/10.1016/j.est.2023.108908

[17] «Chemical potential of different phases inside the pyramid stepped basin solar still through Gibbs free energy», *Case Studies in Thermal Engineering*, vol. 49, p. 103277, Sep. 2023, https://doi.org/10.1016/j.csite.2023.103277

[18] A. F. Abed, M. J. Alshukri, and D. M. Hachim, «Improving solar still performance via the integration of nanoparticle-enhanced phase change materials: A novel pyramid-shaped design with a numerical simulation approach», *Journal of Energy Storage*, vol. 97, p. 112980, Sep. 2024, https://doi.org/10.1016/j.est.2024.112980

[19] X. Wei *et al.*, «Pyramid floating solar still with enhanced condensation surfaces operating under actual weather conditions», *Renewable Energy*, vol. 237, p. 121579, dic. 2024, https://doi.org/10.1016/j.renene.2024.121579

[20] F. A. Essa *et al.*, «Experimental multifaceted approach for enhance pyramidal solar still productivity: Tracking, corrugated absorber, reflectors, external condenser, and phase change material integration», *Process Safety and Environmental Protection*, vol. 197, p. 107061, May 2025, https://doi.org/10.1016/j.psep.2025.107061

[21] N. Mekki, O. Ghriss, A. Bouabidi, K. A. Hammoodi, and S. A. Kadhim, «4 E analysis of pyramid solar still with heat storage using different PCM layer thickness: Energy, exergy, economic, and enviro-economic», *Journal of Energy Storage*, vol. 130, p. 117374, Sep. 2025, https://doi.org/10.1016/j.est.2025.117374

[22] R. Meena *et al.*, «Performance enhancement of pyramid solar still integrated with evacuated tube collector, phase change material, and fins: Thermal, exergy, economic, and environmental analysis», *Journal of Energy Storage*, vol. 127, p. 117094, ago. 2025, https://doi.org/10.1016/j.est.2025.117094

[23] ASHRAE, «OVERALL COEFFICIENT OF HEAT TRANSFER». Accedido: 24 de septiembre de 2025. [En línea]. Disponible en: https://www.aspen.gov/DocumentCenter/View/124/ASHRAE-Fundamentals-Handbook-PDF?bidId=&utm_source=chatgpt.com

[24] M. H. Sharqawy, J. H. Lienhard, and S. M. Zubair, «Thermophysical properties of seawater: a review of existing correlations and data», *Desalination and Water Treatment*, vol. 16, n.º 1, pp. 354-380, April. 2010, https://doi.org/10.5004/dwt.2010.1079

[25] Forest Products Laboratory, «Wood Handbook, Wood as an Engineering Material», *Centennial Edition*, p. 509, 2010.

[26] Styrofoam Brand, «Styrofoam™ Brand Cavitymate™ Ultra XPS Foam Insulation». 2025. Accedido: 24 de septiembre de 2025. [En línea]. Disponible en: https://www.dupont.com/content/dam/dupont/amer/us/en/performance-building-solutions/public/documents/en/styrofoam-brand-cavitymate-ultra-pis-43-D100051-enNA.pdf?utm_source=chatgpt.com

[27] Y. Cengel y A. Ghajar, *Fundamentos y aplicaciones de la transferencia de calor y masa.*, 5.ª ed. Grawhil Education. Accedido: 24 de septiembre de 2025. [En línea]. Disponible en: https://www.scirp.org/reference/referencespapers?referenceid=1875128&utm_source=chatgpt.com

[28] G. N. Tiwari, Md. Meraj, M. E. Khan, R. K. Mishra, and V. Garg, «Improved Hottel-Whillier-Bliss equation for N-photovoltaic thermal-compound parabolic concentrator (N-PVT-CPC) collector», *Solar Energy*, vol. 166, pp. 203-212, May 2018, https://doi.org/10.1016/j.solener.2018.02.058

[29] C. C. Smith y T. A. Weiss, «Design application of the Hottel-Whillier-Bliss equation», *Solar Energy*, vol. 19, n.º 2, pp. 109-113, ene. 1977, https://doi.org/10.1016/0038-092X(77)90047-0

[30] R. Immanual, K. Kannan, N. Sanjana, and K. M. Kirthika, «Performance enhancement of solar still desalination using sound agitation and condensation: A comparative study», *Desalination and Water Treatment*, vol. 321, p. 100923, ene. 2025, https://doi.org/10.1016/j.dwt.2024.100923

[31] A. Ayoobi y M. Ramezanizadeh, «A Detailed Review Investigating the Mathematical Modeling of Solar Stills», *Front. Energy Res.*, vol. 10, abr. 2022, https://doi.org/10.3389/fenrg.2022.879591

[32] A. A. Al-Tabbakh, «Numerical transient modeling of a flat plate solar collector», *Results in Engineering*, vol. 15, p. 100580, Sep. 2022, https://doi.org/10.1016/j.rineng.2022.100580

[33] A. Johnson *et al.*, «A Thermal Model for Predicting the Performance of a Solar Still with Fresnel Lens», *Water*, vol. 11, no. 9, p. 1860, Sep. 2019, https://doi.org/10.3390/w11091860

[34] M. L. Baptista, S. Panse, and B. F. Santos, «Revision and implementation of metrics to evaluate the performance of prognostics models», *Measurement*, vol. 236, p. 115038, ago. 2024, https://doi.org/10.1016/j.measurement.2024.115038

[35] A. Jierula, S. Wang, T.-M. Oh, y P. Wang, «Study on Accuracy Metrics for Evaluating the Predictions of Damage Locations in Deep Piles Using Artificial Neural Networks with Acoustic Emission Data», *Applied Sciences*, vol. 11, n.º 5, p. 2314, ene. 2021, https://doi.org/10.3390/app11052314